Pulsed photothermal radiometry of port-wine-stain lesions

Steven L. Jacques, J. Stuart Nelson, William H. Wright, and Thomas E. Milner

Pulsed photothermal radiometry is used to map the heat deposition in human skin after a short laser pulse. It uses an IR (HgCdTe) detector for a rapid noncontact measurement of the skin surface temperature based on the blackbody emission in the 8–12-μm spectrum. The heat deposited by the laser pulse in the superficial epidermis causes an immediate temperature jump, and the heat deposited in basal epidermal melanin and deep port wine stains diffuses to the surface before detection. The time course of the surface temperature $T(z = 0, t)$, indicates the initial spatial distribution of heat, $T(z, t = 0)$, deposited by the laser.

Key words: Laser, dermatology, IR radiometry, port wine stain.

1. Introduction

The challenge of many medical laser applications is to understand radiative transport in complex tissues in order to aid the physician in the design of therapeutic protocols. How the laser's radiant energy propagates through a tissue and deposits heat often determines the therapeutic effect of the procedure. Port-wine-stain (PWS) therapy uses a pulsed dye laser to deposit heat selectively into these vascular abnormalities to cause irreversible thermal injury, which elicits a wound-healing response that clears the PWS. Selective absorption of the laser radiation, usually at 577 or 585 nm, by hemoglobin saves the overlying epidermis and surrounding dermis from injury. However, the ability of light to penetrate to deep PWS's is restricted by epidermal melanin at the skin surface, which filters light, and by dermal scattering, which inhibits deep light penetration. The PWS structure is quite variable from patient to patient and from site to site with both superficial and deep lesions. The physician faces a laser dosimetry problem in which differences in laser energy delivery cause the efficacy of the therapy to vary. A measurement that could specify the distribution of deposited laser energy in the PWS of specific skin sites would provide the best aid to the physician in managing clinical laser protocols.

Pulsed photothermal radiometry (PPTR) uses an IR detector to monitor skin surface temperature after a laser pulse, thereby providing information on deducing the internal distribution of deposited heat.[1–4] Heat deposited at the surface causes an immediate rise in temperature; heat deposited deeper within the tissue must diffuse to the surface before detection is possible. The deeper the laser energy deposition, for example, in a deep PWS, the longer the delay before the heat reaches the surface and affects the detected surface temperature. Therefore the time course of the laser-induced surface temperature rise, $T(z = 0, t)$, above the ambient skin temperature can specify the initial spatial distribution of heat, $T(z, t = 0)$, immediately after the laser pulse.

This paper outlines the PPTR method both theoretically and experimentally. PPTR measurements of the surface temperature after pulsed 577-nm laser irradiation of the chicken hen comb illustrate how a tissue's blood content affects the signal. Measurements of human skin sites after irradiation by both the 577-nm dye laser and the 694-nm ruby laser illustrate the relative contributions of epidermal melanin and a deeper PWS to the PPTR signal. An algorithm for deducing $T(z, t = 0)$ from $T(z = 0, t)$ is presented and applied to a human PWS.

2. Materials and Methods

A. Pulsed Photothermal Radiometry

The PPTR apparatus is shown in Fig. 1. A HgCdTe detector (Model MPC11-2-A1, New England Re-

S. L. Jacques is with the Laser Biology Research Center, M. D. Anderson Cancer Center, University of Texas, Houston, Texas 77030. The other authors are with the Beckman Laser Institute and Medical Clinic, University of California, Irvine, Irvine, California 92715.

Received 6 February 1992.
0003-6935/93/132439-08$05.00/0.

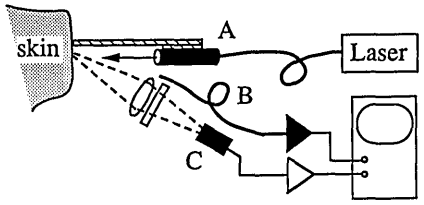

Fig. 1. Pulsed photothermal radiometry apparatus. The device measures the blackbody emission from a skin site to indicate the surface temperature as a function of the time following irradiance by a pulsed laser. A, a ruby or dye laser delivers a 3-J/cm^2 laser pulse through an optical fiber whose terminus is imaged by a lens (within a black cylinder) onto the skin site as a 5-mm-diameter uniform beam. Two rods (one is shown) positions the skin site exactly at the proper position relative to the lens systems. B, an optical fiber collects reflected light for detection by a photodiode whose output passes to a digital oscilloscope. C, the central 2-mm region of the irradiated skin site is imaged by a germanium lens through a long-pass filter (>7.5 μm) onto a HgCdTe detector whose signal is amplified before it passes to the oscilloscope. The angle between the laser beam axis and IR collection axis is ~20°.

search Center, Sudbury, Mass.), cooled by liquid nitrogen, was used in all experiments. The device had a 2 × 2-mm^2 detector area that viewed a similar area on the skin site by 1:1 imaging with a germanium lens. A long-pass filter (with a >7.5-μm wavelength) blocked any stray visible or near-IR radiation from reaching the detector. The detector was a photoconductor connected as one arm of a Wheatstone bridge. The signal across the bridge was amplified by a battery-powered, high-gain, low-noise, 2.5-kHz-bandwidth, differential, dc amplifier. The amplified signal was acquired by a digitizing oscilloscope (Model DSA 601, Tektronix, Beaverton, Ore.), which communicated with a personal computer (Macintosh, Apple Computers Inc., Calif.) by a GPIB interface controlled by LabVIEW software (National Instruments, Austin, Tex.).

A flash-lamp-pumped dye laser (Model SPTL-1, Candela, Wayland, Mass.) delivered a 588-mJ, 360-μs pulse of light at a 577-nm wavelength to the skin site through an optical fiber with a lens system. The irradiance was uniform and covered a circular spot that was 5 mm in diameter, which yielded a radiant exposure of 3 J/cm^2. Although the laser energy can be adjusted up to 10 J/cm^2 for treatment, the lower radiant exposure was sufficient for the diagnostic PPTR measurement. The detector viewed the central 2-mm zone of the irradiance spot. In some experiments a ruby laser was used to deliver a 500-μs pulse at 3 J/cm^2. We positioned both the dye and ruby lasers to permit alternate irradiation with each laser on the same skin site. The PPTR system was rigidly assembled on a square platform [0.0929 m^2 (~1 ft^2)] that was held by an adjustable arm for the convenient positioning near the patient.

Calibration of the HgCdTe detector–lens system was obtained by measurements of a block of graphite at 24°C (room temperature) and 31°C (heated in a water bath, then dried). Temperatures were confirmed by a quartz temperature probe (Model 10023A, Hewlett Packard, Palo Alto, Calif.). Measurements of forearm skin, also at 31°C, yielded the same PPTR signal as the heated graphite did because both emissivities are close to one; therefore we adopted the following routine method of calibration. Measurements of the 24°C graphite block and the 31°C forearm, both verified by a thermocouple, yielded a 1.10-V difference in the PPTR signal as recorded by the oscilloscope after preamplification; therefore the calibration was 6.35°C/V. The noise level for the measurement was ~10 mV or 0.06°C. Although the detected blackbody emission is proportional to T^4, at a high absolute temperature a linear response is expected. When the PPTR system was used, the response was essentially linear for the few degrees of temperature rise.

We acquired optical measurements of diffuse reflectance by collecting light with an optical fiber. Diffuse reflectance is light that has entered the tissue and has been backscattered by the tissue-scattering properties. Specular reflectance is light that has never entered the skin but rather has been reflected by the air–skin interface. We placed the collection fiber off axis normal to the skin to avoid the collection of specular reflectance from the skin; however, because of skin roughness the measurement did contain a small amount of specular reflectance. We calibrated the collection efficiencies of the fiber and the detector response by measuring reflectance from a known standard (Spectralon, 99.4%; Labview, Inc., North Sutton, N.H.).

In this prototype PPTR system our recent experiments demonstrate that the initial temperature rise includes a transient contribution caused by absorption by the germanium lens of backscattered light from the tissue. The absorption of the laser light by the germanium lens is strong with an absorption coefficient of 3.8 × 10^5 cm^{-1} at a 585-nm wavelength. The thermal diffusivity of germanium (0.3 cm^2/s) is high and thermal relaxation is rapid. The lens heating closely follows the laser pulse and affects the first 500 μs of the signal. We are currently redesigning the lens system so that it avoids such an artifact.

B. Chicken Comb Experiments

The combs of two adult female Leghorn chickens weighing 2.5–3.5 kg were measured by PPTR after irradiation with the pulsed dye laser (3 J/cm^2). One chicken was younger and the comb appeared to be a light red; the other chicken was older and the comb appeared to be dark red. The highly vascularized comb was used as an animal model because its histoanatomy is analogous to that found in PWS and because it has been studied extensively by the authors.[5] Pulsed laser radiation can achieve blanching of the comb's blood vessels that is similar to the blanching of PWS in humans. Experimental protocols and the handling of animals were approved by the Animal Research Committee at the University of California, Irvine, Calif.

C. Human PWS Experiments

Human subjects were recruited from the patient population currently receiving PWS therapy at the Beckman Laser Institute and Medical Clinic. Permission for the study was obtained from the Institutional Review Board Human Subjects Review Committee at the University of California, Irvine, Calif. The subjects were supine on an adjustable electromechanically controlled hospital bed during the measurements with the PPTR apparatus positioned near the arm, shoulder, or face. The patients received a radiant exposure of 3 J/cm^2, which is below the therapeutic exposure of 5–10 J/cm^2. During all the experiments the patients wore eye protection.

3. Results

A. Hen Combs

In Fig. 2 we show the measurements on two hen combs, one light red and the other dark red because of differences in the tissue blood content. In Figs. 2A and 2B we depict measurements on different tissue sites and different time scales. In Fig. 2A we show the early response. Since the chicken comb does not have epidermal melanin, the initial temperature rise should not be interpreted as the heating of epidermal melanin. The rise is due to heating of the nonpigmented epidermis, and the artifact of germanium lens heating by backscattered light as discussed in Section 2. The signal caused by lens heating was a transient signal that decayed in ~1 ms. The arrows in Figs. 2–4 indicate the estimated temperature rise caused by the epidermis without lens heating when the first millisecond of data is ignored. After the immediate temperature rise, both combs showed a delayed temperature rise because of the blood vessels that absorbed laser energy. The time delay corresponded to the diffusion of heat from the vessels within the skin to the surface where the temperature was detected.

In Fig. 2B we show the responses on a longer time scale. Because of the larger thermal deposition in the dark comb compared with the light comb, the dark comb showed a greater delayed surface temperature rise. The delayed temperature rise for both combs peaked at ~30 ms, which is consistent with a similar blood vessel distribution for both combs located at an ~80-μm depth. Therefore the PPTR signals indicated that, although the dark and light combs differed in size and/or concentration of blood vessels, their spatial distribution was similar. The relationship between the time delay and the depth of a PWS is presented in Section 4.

B. Human Normal versus the PWS

In Fig. 3 we compare measurements of the surface temperature of a normal site and a PWS with similar but not exactly equal epidermal pigmentation. In both cases the initial surface temperature rise was ~3°C because the laser heated the pigmented epidermis. The arrows indicate the estimated initial temperature rise without the artifactual lens heating. With time the surface temperature of the normal skin site decreased. In contrast, although the surface temperature for the PWS decreased at first, it increased again as the heat initially deposited in the PWS reached the surface. The delayed temperature

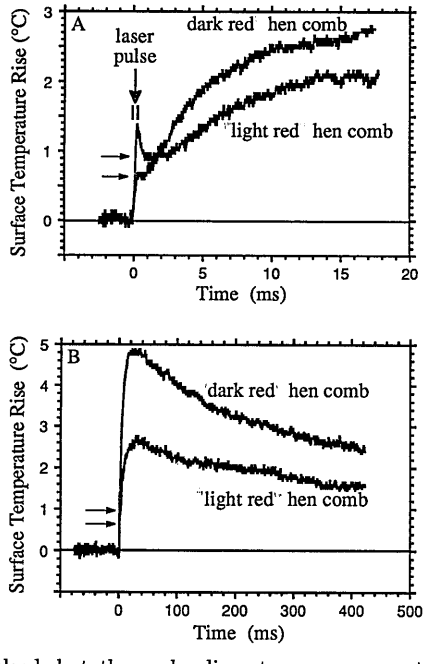

Fig. 2. Pulsed photothermal radiometry measurements of chicken hen combs, one light red and one dark red. A, the early response occurs in the first 20 ms. (B) the later response occurs in over 400 ms. (A and B are on different tissue sites). The dye laser at 577 nm irradiates the combs and is absorbed by the blood vessels. The dark comb absorbs more light and shows a greater temperature rise. The delayed temperature rise peaks at ~30 ms, which is consistent with the location of the first blood vessels at an ~80-μm depth. Arrows indicate the initial temperature rise of the epidermis without the transient artifact of lens heating, which contributes to the first millisecond of the signal.

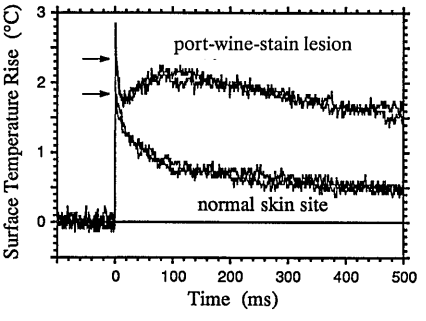

Fig. 3. Comparison of the normal site and the PWS. The 577-nm dye laser (with a 3-J/cm^2 exposure) irradiates a normal skin site and a PWS. The initial temperature jump is caused by the absorption of light by the pigmented epidermis. The arrows indicate the initial temperature rise of the epidermis without the transient artifact of lens heating, which contributes to the first millisecond of the signal. The delayed temperature rise seen for the PWS is due to the laser deposition of energy in the blood vessels of the PWS, which must diffuse to the surface before detection. The delayed temperature rise peaks at ~100 ms, which is consistent with the location of the PWS at a 150-μm depth.

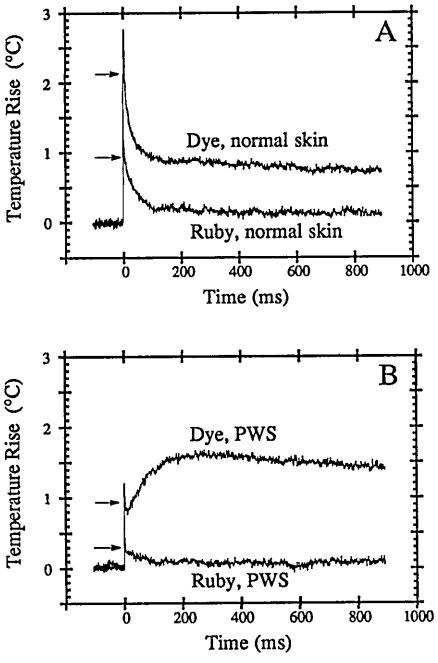

Fig. 4. Comparison of ruby and dye laser exposures: A, normal skin site; B, PWS. Since the 577-nm dye laser is more strongly absorbed by epidermal melanin than the 694-nm ruby laser, the dye laser causes a greater initial temperature jump. The dye laser irradiation of the PWS causes a delayed temperature rise as heat deposited in deep blood arrives at the surface at ~300 ms, which is consistent with the location of the PWS at an ~260-μm depth. However, the ruby laser does not efficiently heat blood, and no delayed temperature rise is obvious. The arrows indicate the initial temperature rise of the epidermis without the transient artifact of lens heating that contributes to the first millisecond of the signal.

rise peaked at ~100 ms, which is consistent with the PWS being located at a depth of ~150 μm.

C. Human PWS with Ruby Versus Dye Lasers

In Fig. 4 we show the measurements on human normal sites and the PWS by using the ruby versus dye lasers. In Fig. 4A we show the temperatures on a normal site after ruby or dye laser exposures. The normal site was well pigmented, and the immediate temperature rise dominated the measurement. The 694-nm wavelength of the ruby laser is less strongly absorbed by epidermal melanin, dermis, and blood and is less strongly scattered by the dermis than is the 577-nm wavelength of the dye laser.[6,7] Therefore the ruby laser pulse elicited a temperature rise that was less than the dye laser pulse. In Fig. 4B we show the measurements on a PWS. The temperature rises were lower as a result of less epidermal melanin at the PWS site, but the dye laser still caused a greater temperature rise than the ruby laser did. Reflectances of the dye laser were 0.38 and 0.22 for normal and PWS, respectively; the reflectances of the ruby laser were 0.67 and 0.65 for normal and PWS, respectively. These reflectances indicate that the dye laser, not the ruby laser, was strongly absorbed by the blood of the PWS. Also, there was a delayed arrival of heat from the deep PWS after irradiation with the dye laser; the arrival time of the peak was ~300 ms, which implied a PWS depth of ~260 μm. The yellow light of the dye laser effectively heated the blood of the PWS, but the red light of the ruby laser did not.

4. Discussion

A. Pulsed Photothermal Radiometry Theory

Two aspects of the PPTR signal are of interest: (1) the initial temperature rise because of the immediate heating of the pigmented epidermis and (2) the delayed arrival of heat at the surface because of the heating of a buried PWS.

The radiant exposure ϕ_0 in J/cm^2 is delivered to the skin surface. However, the skin backscatters a significant fraction of the light. Backscattered light also heats the pigmented epidermis. The initial temperature rise experienced by the skin surface is

$$\Delta T = \frac{\mu_a \phi_0 (1 + 6.7R)}{\rho C}, \tag{1}$$

where μ_a is the absorption coefficient in cm^{-1}, R is the diffuse reflectance, ρ is the tissue density, and C is the specific heat. The factor of 6.7 is approximately correct for skin with a refractive index of 1.37. The factor depends on the mismatch in the refractive indices of the tissue and the air.[1] Diffusion theory would predict a factor of 6.35. More careful Monte Carlo simulations indicate that the anisotropy of specific radiance near a mismatched boundary increases internal reflectance and yields a factor of 7.1.[8] The roughness of the surface complicates the problem, and a factor of 6.7 is assumed here until a more accurate treatment is conducted. The values of ρ in g cm^{-3} and C in J g^{-1} °C^{-1} can be approximated according to the water content W of the tissue[9]:

$$\rho = (1.3 - 0.3W), \tag{2}$$

$$C = 4.18(0.37 + 0.67W/\rho). \tag{3}$$

If W equals 0.75 g of water/g of total tissue, the values of ρ and C are 1.07 g cm^{-3} and 3.50 J g^{-1} °C^{-1}, and the term ρC equals 3.76 J cm^{-3} °C^{-1}.

Consider a typical PPTR measurement of skin at a 577-nm wavelength. The optical properties of tissue are the absorption coefficient μ_a and the scattering coefficient μ_s in cm^{-1} and the anisotropy of scattering g (dimensionless). For a nonpigmented skin site the approximate values of dermal optical properties at 577 nm are $\mu_a = 0.8$ cm^{-1}, $\mu_s = 120$ cm^{-1}, and $g = 0.8$.[7,10] The optical penetration depth δ of diffusion theory is

$$\delta = \frac{1}{\{3\mu_a[\mu_a + \mu_s(1 - g)]\}^{1/2}}. \tag{4}$$

Therefore δ equals 0.13 cm. The diffuse reflectance from a tissue is approximately[11]

$$R = \exp(-7\delta\mu_a). \quad (5)$$

Therefore $R = 0.48$. If the PPTR measurement uses a radiant exposure ϕ_0 of 3 J/cm^2, Eq. (1) predicts that the resulting initial temperature rise ΔT would equal 2.7°C.

The theory described above and in the following subsection is one dimensional. The irradiance must be uniform, and the spot size must be sufficiently large for us to achieve a one-dimensional optical/thermal transport problem in the central 2-mm-diameter zone viewed by the HgCdTe detector. As a rule of thumb the diameter of the spot size should exceed at least 4δ for it to approach the maximal reflectance in the central region of the irradiance spot; in this case the measured R_d will correspond to the maximal R_d in the central region of irradiance. If $\delta = 1.3$ mm, then $4\delta = 5.2$ mm. Therefore to allow for a central region of 2 mm, which conforms to the one-dimensional theory, we should choose a laser spot that is at least 7.2 mm in diameter. Because our 5-mm-diameter laser spot was slightly too small, the local reflectance in the central spot viewed by the HgCdTe detector will be slightly lower than the R_d deduced from the optical fiber measurements. Therefore in Eq. (1) ΔT is slightly underestimated in these experiments. In future work a larger spot size should be used.

B. Algorithm for Mapping the Temperature Rise

The second aspect of the PPTR signal is the delayed arrival of heat at the surface, which indicates the depth of the PWS. A simple algorithm was implemented to convert the time course of the surface temperature rise, $T(z = 0, t)$, into the spatial distribution of the initial laser-induced temperature rise, $T(z, t = 0)$.[12] Recently Prahl[13] developed a conversion method based on matrix manipulations that may improve our simple algorithm. Our algorithm does all the bookkeeping in units of temperature (°C), although alternatively one may use energy density (J/cc). The algorithm is based on a one-dimensional impulse response or Green's function (G) for the thermal diffusion of heat at distance z at time t from an impulse of heat deposition. Consider first the general expression for $G(z, t)$ in an infinite medium with no boundary conditions:

$$G(z, t) = \frac{\exp(-z^2/4kt)}{2(\pi kt)^{1/2}}. \quad (6)$$

When we expand[14] to the case of heat diffusion from a layer of deposited heat with width w,

$$G(z, w, t) = \frac{1}{2}\left\{\mathrm{erf}\left[\frac{z + w/2}{(4kt)^{1/2}}\right] - \mathrm{erf}\left[\frac{z - w/2}{(4kt)^{1/2}}\right]\right\}, \quad (7)$$

where erf is the error function; G is dimensionless. At time zero the value of $G(z \pm w/2, w, 0)$, which corresponds to the edges of the heated layer, equals unity. However, at an incremental time immediately after the impulse the value of $G(z \pm w/2, w, t)$ is 0.5. The k factor is the thermal diffusivity that is approximated by

$$k = (0.133 + 1.36W/\rho)(10^{-3}) \quad (8)$$

in units of cm^2/s, which equals 1.08 cm^2/s for $W = 0.75$ g of water/g of total tissue.

The temperature rise at a distance z from the center of the heated layer is related to the product of $G(z, w, t)$ and the temperature rise $T(0, 0)$ of that heated layer:

$$T(z, t) = G(z, w, t)T(0, 0). \quad (9)$$

Now consider the case of a semi-infinite medium with a surface boundary condition. For skin exposed to air, the surface serves as an insulating boundary on the short time scale of the PPTR measurements. The few degrees of temperature rise are not expected to elicit significant convective or radiative losses within the 1-s measurement period, and the low water content and low water permeability of the skin surface do not permit significant evaporative cooling. The thermal diffusion problem with an insulating boundary is solved by the method of images. The origin, $z = 0$, is aligned with the tissue surface, and the positive z refers to the depth of the heated layer's center. The region of air above the semi-infinite tissue, $z < 0$, is replaced by tissue to create an infinite homogeneous tissue, and an image source of heated tissue layer is placed at $z_{\mathrm{image}} = -z$. The superposition of the responses at the surface to the original source and the image source simply adds a factor of 2 to Eq. (7). Therefore the net impulse response of the surface to a layer of heated tissue centered at depth z for the case of a semi-infinite tissue with an insulated surface boundary is

$$G(z, w, t) = \mathrm{erf}\left[\frac{z + w/2}{(4kt)^{1/2}}\right] - \mathrm{erf}\left[\frac{z - w/2}{(4kt)^{1/2}}\right]. \quad (10)$$

For the case of a layer of width w centered at depth $z = w/2$, the heated layer extends to the tissue surface. At time zero the value of $G(0, w, 0)$, which corresponds to the surface temperature, is two, which is erroneous, and Eq. (10) should not be applied at time zero. However, at an incremental time immediately after the impulse, the value $G(0, w, t) = 1$, which is correct. At longer times, $G(0, w, t)$ will decrease as heat diffuses into the tissue.

The algorithm considered N discrete tissue layers denoted by the index j, which were heated by the laser pulse to yield a temperature rise T_j. Each jth layer had a position z and a width w and the surface temperature rise, $T(z = 0, t)$, because of heating from each jth layer was given by $G(z, w, t)T_j$, which we refer to as $G_j(t)T_j$ for simplicity. The temperature rise

because of all the N heated layers is

$$T(z = 0, t) = \sum_{j=1}^{N} G_j(t)T_j. \quad (11)$$

The width w of the discrete layers of heating was chosen to equal 15 μm. The position z referred to the center of a particular tissue layer. The values for z_j were

$$z_j = (j - 0.5)w. \quad (12)$$

In Fig. 5 we illustrate the application of the algorithm in the analysis of a typical PPTR measurement, $T(z = 0, t)$ or simply $T(t)$, on a human PWS. The original $T(t)$ signal is shown as the uppermost envelope of the signal trace in Fig. 5A. Before we applied the algorithm, the artifactual temperature rise caused by lens heating was removed by rejecting the first millisecond of data, and a smoothing algorithm averaged data within ±2 ms of each time point to eliminate unnecessary noise.

The basis idea of the algorithm is to attribute the earliest temperature rise to the heating of the most superficial layer of heated tissue T_1. Then the contribution of T_1 to all subsequent times can be predicted by $G_1(t)T_1$. The difference between measurement and prediction, in other words $T(t) - G_1(t)T_1$, indicates the temperature rise that must be a result of the next layer of heating T_2. The contribution of T_2 to all subsequent times can be calculated by $G_2(t)T_2$. The difference $T(t) - G_1(t)T_1 - G_2(t)T_2$ indicates the temperature rise that must be the result of the next layer of heating T_3. The algorithm progressively deduces the T_j for the jth layer of tissue heating based on the difference between the measured signal $T(t)$ and the accumulated predicted signal based on the heating of the first $j - 1$ layers.

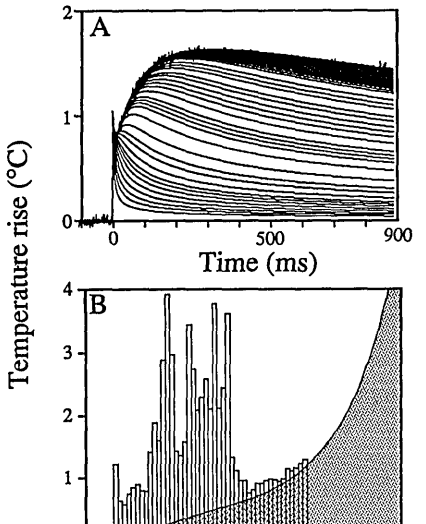

Fig. 5. Deducing the initial spatial distribution of heat deposition from the time course of the surface temperature. An algorithm for converting $T(z = 0, t)$ into $T(z, t = 0)$ is demonstrated. A, the measured surface temperature $T(z = 0, t)$ is the upper envelope of the signal trace. The curves that accumulate under the signal are the plots of the accumulated prediction $M_j(t)$ of the temperature time course based on the heating of the first j layers that the algorithm has progressively deduced. As j proceeds from 1 to N, $M_j(t)$ approaches the measurement envelope $T(z = 0, t)$. B, the deduced distribution $T(z, t = 0)$ equals the temperature rise T_j deduced for layers j = 1–N [see the algorithm, Eqs. (13)–(16)]. The solid curve at the upper bound of the hatched area indicates the error in the predicted $T(z, t = 0)$ that occurs as a result of the signal noise and the noise limit of 0.01°C used by the algorithm to discriminate $T(t) - M_j(t) >$ noise. The solid curve equals (0.01°C)/[maximum value of $G_j(t)$]; see Section 4.

The algorithm can be summarized by the following programming statements, which apply to N layers of heated tissue:

$$T_1 = T(t)/G_1(t). \quad (13)$$

For $j = 1$ to $N - 1$ do the following:

Begin

$$M_j(t) = \sum_{k=1}^{j} G_k(t)T_k, \quad (14)$$

$$\Delta_{j+1}(t) = T(t) - M_j(t), \quad (15)$$

$$T_{j+1} = \text{minimum value of } \Delta_{j+1}(t)/G_{j+1}(t) \text{ over the measurement period where } \Delta_{j+1}(t) > \text{noise} \quad (16)$$

End.

In the above algorithm Eq. (13) initiates the analysis by deducing the temperature rise of the first layer T_1. Then the do-loop indicated by Eqs. (14)–(16) iteratively deduces the temperature rise T_{j+1} for the $j + 1$ layer. First, Eq. (14) accumulates the predicted temperature time course $M_j(t)$ based on the heating attributed to the first j layers, which is essentially the same as in Eq. (11). Second, in Eq. (15) we calculate the difference $\Delta_{j+1}(t)$ between the actual measurement and the accumulated prediction $M_j(t)$. Third, Eq. (16) assigns to T_{j+1} the minimum value of $\Delta_{j+1}(t)/G_{j+1}(t)$ encountered over the time course subject to the condition that $\Delta_{j+1}(t)$ is positive and exceeds the noise limit of the algorithm. The noise limit was set to be equal to 0.01°C for this algorithm. The condition $\Delta_{j+1}(t) >$ noise caused the algorithm to search forward in time until the difference between the measurement and accumulated prediction became significant. Choosing the minimum value of $\Delta_{j+1}(t)/G_{j+1}(t)$ caused the algorithm to favor the data from the time when $G_{j+1}(t)$ was maximum, in other words the time when the peak surface temperature rise would occur because of the $j + 1$ layer. The net result of the algorithm was the gradual accumulation of $M_j(t)$ under the measurement envelope $T(t)$. The series of $M_j(t)$ for $j = 1 \ldots N$ is shown in Fig. 5A.

The arrival time for the peak of the delayed temperature rise was ~30 ms for chicken combs, as shown in

Fig. 2B. The peak arrival times for the PWS were ~100 ms in Fig. 3 and ~300 ms in Fig. 4. We can calculate the time of arrival of the peak caused by heat deposition in a layer centered at a depth z by using Eq. (7). The results of such a calculation can be summarized by the following expression relating the arrival time of the peak t_{peak} in seconds and the depth of the layer z in centimeters:

$$z = 0.0466 t^{1/2}. \quad (17)$$

A PWS is usually distributed and is not accurately assigned to one particular depth. Equation (17) simply offers an estimate of where most of the laser energy is deposited. According to Eq. (17), the peak arrival times of ~30, 100, and 300 ms imply PWS depths of 80, 150, and 260 μm, respectively.

The surface temperature rise in Fig. 5A did not exceed ~1.3°C. However, at depths of approximately 200–400 μm the internal temperatures indicated in Fig. 5B reached ~4°C. These temperatures, however, were based on the average temperature in a heated layer and assumed that the PWS structure could be modeled as a one-dimensional structure with the variation as only a function of depth. If the assumption is correct, indeed the PWS temperature is raised by 4°C. In reality, however, the PWS at a given depth may not be uniform in the $x - y$ plane under the measurement area and the one-dimensional assumption would be incorrect. The density of PWS in the dermis may be relatively low, for example, perhaps only 10% of the dermal volume. The PWS is filled with whole blood, but the surrounding dermis has only a low blood content because of normal vessels. The 4°C temperature rise corresponds to the average heating of the PWS and the surrounding dermis at a particular depth. As the heat diffuses to the surface, the heat from the PWS and surrounding dermis will mix to some degree. The PPTR measurement at the surface yields an average value of temperature over the measurement area. Between thermal mixing during diffusion and signal averaging during measurement, the PPTR cannot distinguish the details of the PWS structure. Therefore the actual temperature rise of the PWS may be higher, perhaps as much as 10-fold higher, than is indicated in Fig. 5B. It may be somewhere in the range of 4–40°C. The interpretation of PPTR measurements at the surface in terms of initial PWS temperatures is ambiguous when the PWS at a given depth is not uniform in the $x - y$ plane under the measurement area.

If a 6-J/cm² therapeutic exposure was delivered, rather than the 3-J/cm² diagnostic exposure of the PPTR measurement in Fig. 5, the temperature rise of the PWS would have been in the range of 8–80°C, which would yield a final temperature of 39–111°C (an initial skin temperature of ~31°C). If one assumes that the threshold temperature that a PWS must achieve to yield a therapeutic effect is ~100°C and assumes that 6 J/cm² is the threshold exposure for efficacy for this particular PWS, the PPTR measurement in Fig. 5B would suggest that the estimate that the PWS constitutes ~10% of the dermal volume in the 200–400-μm range is reasonable.

In Fig. 5B the radiant exposure was 3 J/cm², the optical reflectance was 0.22, and the epidermal temperature rise was in the range of 0.5–1.3°C or ~1°C. Therefore the average absorption coefficient of the pigmented epidermis can be calculated by using Eq. (1):

$$\mu_a = \frac{\Delta T \rho C}{\phi_0(1 + 6.7R)} = \frac{(1°C)(3.76\ J/cm^3\ °C)}{(3\ J/cm^2)[1 + 6.7(0.22)]} = 0.5\ cm^{-1}. \quad (18)$$

The value of 0.5 cm^{-1} for μ_a is in general agreement with recent integrating sphere studies of skin optical properties that indicate that $\mu_a = 0.8\ cm^{-1}$ at 577 nm for human neonatal skin[10] with negligible melanin pigment and 0.3 cm^{-1} for hairless rat skin (unpublished results).

C. Sources of Error

Heating of the germanium lens by reflected light contributed a transient impulse to the initial temperature rise, as mentioned in Sections 2 and 3. We are devising a new lens system that avoids this effect.

The analysis algorithm described in this paper is too simple and subject to error. The analysis in Fig. 5B was specified by a single pass with the algorithm through the N layers of heating. During one pass, however, the early $T(t)$ yields predictions for the first few T_j, i.e., $j = 1, 2, 3$, etc., which do not anticipate that subsequent T_j may also contribute slightly but significantly to the early $T(t)$. The result is an overestimate of the first few T_j values. An iterative algorithm is needed to readjust the first pass of predicted T_j values. Prahl[13] developed such an algorithm based on matrix operations, which is expected to achieve proper values for T_j. Nevertheless the simple algorithm presented in this paper outlines and Fig. 5 illustrates the basic principles of any analytic method.

Another source of error was signal noise. The algorithm relied on a noise limit of 0.01°C as it sought the minimum value of $\Delta j(t)/G_j(t)$, where $\Delta j(t) >$ noise [Eq. (16)]. Therefore a systematic error corresponding to the minimum value of $(0.01°C)/G_j(t)$ was expected in the predicted value of T_j. The solid curve at the upper bound of the hatched area in Fig. 5B illustrates this error; the solid curve equals $(0.01°C)/[\text{maximum value of } G_j(t)$ during the measurement period]. The error increases linearly over the first 500 μm, then grows rapidly at deeper depths.

Another source of error was involuntary patient movement during the measurement. Although the PPTR measurement recorded surface temperature over <1 s, patient movements such as breathing and slight twitching sometimes contributed to slight fluctuations in measured $T(z = 0, t)$, which yielded large

errors in predicted T_j, especially for deeper layers. One improvement in the PPTR measurement that we recently implemented is a PPTR system using three optical fibers, one for the pulsed laser, one for the collection of reflectance, and a third IR-transmissive fiber to carry collected IR emission to the HgCdTe detector. The PPTR system becomes a handheld device that facilitates placement on the patient and may reduce the effects of involuntary patient movement.

5. Summary

The PPTR system offers a method for specifying initial heat deposition by a pulsed laser in complex tissue such as a PWS. The physician learns the degree of epidermal heating that will occur with pulsed irradiation and therefore can avoid or at least be prepared for epidermal injury. The physician learns information related to the depth, distribution, and concentration of the blood vessels that constitute a PWS. Such data can guide planning of the clinical protocol and can aid in the discussion of patient treatment.

The study was supported by grants from the National Institutes of Health (R29-45045) and the U.S. Department of Navy (N00014-91-J-4065 and N00015-91-J-1354) to S. L. Jacques and by a Whitaker Foundation Biomedical Engineering Research Grant and Dermatology Foundation Career Development Award and a National Institutes of Health Biomedical Research Technology Program grant (R03-RR06988-01) to J. S. Nelson. The authors thank Michael W. Berns for providing the support facilities and personnel at the Beckman Laser Institute and Medical Clinic.

References

1. R. R. Anderson, H. Beck, U. Bruggemann, W. Farinelli, S. L. Jacques, and J. A. Parrish, "Pulsed photothermal radiometry in turbid media: internal reflection of backscattered radiation strongly influences optical dosimetry," Appl. Opt. **28,** 2256–2262 (1989).
2. F. H. Long, R. R. Anderson, and T. F. Deutsch, "Pulsed photothermal radiometry for depth profiling of layered media," Appl. Phys. Lett. **51,** 2076–2078 (1987).
3. W. P. Leung and A. C. Tam, "Techniques of flash radiometry," J. Appl. Phys. **56,** 153–161 (1984).
4. A. C. Tam and B. Sullivan, "Remote sensing application of pulsed photothermal radiometry," Appl. Phys. Lett. **47,** 333–335 (1983).
5. J. S. Nelson, A. Orenstein, L. H. Liaw, S. Kimel, and M. W. Berns, "Photodynamic therapy of hypervascular cutaneous tissues in animal models using porphyrin or phthalocynanine activated by red light," in *Laser Surgery: Advanced Characterization, Therapeutics, and Systems II,* S. N. Joffe and K. Atsomi, eds., Proc. Soc. Photo-Opt. Instrum. Eng. **1200,** 154–163 (1990).
6. M. J. C. van Gemert, S. L. Jacques, H. J. C. M. Sterenborg, and W. M. Star, "Skin optics," IEEE Trans. Biomed. Eng. **36,** 1146–1154 (1989).
7. S. L. Jacques, "The role of skin optics in diagnostic and therapeutic uses of lasers," in *Lasers in Dermatology,* R. Steiner, R. Kaufmann, M. Landthaler, and O. Braun-Falco, eds. (Springer-Verlag, Berlin, 1991), Chap. 1, p. 1.
8. S. L. Jacques, "Simple theory, measurements, and rules of thumb for dosimetry during photodynamic therapy," in *Photodynamic Therapy: Mechanisms,* T. J. Dougherty, ed., Proc. Soc. Photo-Opt. Instrum. Eng. **1065,** 100–108 (1989).
9. A. N. Takata, L. Zaneveld, and W. Richter, "Laser-induced thermal damage in skin," Rep. SAM-TR-77-38 (U.S. Air Force School of Aerospace Medicine, Brooks Air Force Base, Tex., 1977).
10. I. S. Saidi, "Transcutaneous optical measurement of hyperbilirubinemia in neonates," Ph.D. dissertation (William March Rice University, Houston, Tex., 1992).
11. S. L. Jacques, "Simple optical theory for light dosimetry during PDT," in *Optical Methods for Tumor Treatment and Detection: Mechanisms and Techniques in Photodynamic Theory,* T. J. Dougherty, ed., Proc. Soc. Photo-Opt. Instrum. Eng. **1645,** 155–165 (1992).
12. S. L. Jacques, W. A. Farinelli, F. H. Long, T. F. Deutsch, and R. R. Anderson, "The spatial distribution of optical energy in tissue deduced from IR radiometry of surface temperature after pulsed radiation," presented at the Second European Congress of Photobiology, Padua, Italy, 1987.
13. S. A. Prahl, I. A. Vitkin, U. Bruggerman, B. C. Wilson, and R. R. Anderson, "Determination of optical properties of turbid media using pulsed photothermal radiometry," Phys. Med. Biol. **37,** 1203–1217 (1992).
14. M. Abromowitz and I. A. Stegun, *Handbook of Mathematical Functions* (Dover, New York, 1972), p. 303, Eq. (7.4.32).